© 2014. Published by The Company of Biologists Ltd | The Journal of Experimental Biology (2014) 217, 964-973 doi:10.1242/jeb.092577

RESEARCH ARTICLE

Testing the constant-volume hypothesis by magnetic resonance imaging of *Mytilus galloprovincialis* heart

Eriko Seo[1], Kazue Ohishi[2], Tadashi Maruyama[2], Yoshie Imaizumi-Ohashi[3], Masataka Murakami[4] and Yoshiteru Seo[3,*]

ABSTRACT

The constant-volume (CV) hypothesis was tested using the *Mytilus galloprovincialis* heart under two conditions. The volume of the ventricle, auricles and pericardium, and the flow in the heart and adjacent vessels were measured by magnetic resonance imaging. In synthetic seawater at 23°C (immersed condition), the end-diastolic volume (EDV), end-systolic volume (ESV) and stroke volume (SV) were 50%, 21% and 29% of the heart volume, respectively, and the auricle volume (V_A) was maximized at end-systole. Assuming a constant volume of the heart, venous return to the auricles (I_V) was constant, and out-flow from the pericardium to the kidney (I_{PK}) was 2/3 of SV. During aerial exposure (emersed condition), EDV, ESV and SV decreased to 33%, 22% and 11%, respectively. V_A was maximized at end-diastole and associated with the decrease of systolic I_V to 1/2 of diastolic I_V, while I_{PK} remained at 80% of the immersed condition. Based on these results – in addition to two postulates of the CV hypothesis: (1) the total volume of the heart is always the same, and (2) ventricle contraction causes a decrease in pressure in the pericardium – we modified two postulates: (3) the low pericardial pressure maintains venous return from the anterior oblique vein to the auricle, and (4) the pressure difference between the auricle and the pericardium drives haemolymph filtration through the auricle walls. We also added a new postulate: (5) dilatation of the ventricle is associated with the haemolymph output to the kidney via the renopericardial canals.

KEY WORDS: Cardiac cycle, Heart rate, Haemolymph flow, Stroke volume, Ejection fraction, Renocardiovascular system, Bivalve

INTRODUCTION

The physiology of the hearts of bivalve molluscs has been studied for many years (Bayne, 1976; Beninger and Le Pennec, 2006). Filling of the heart was explained by the constant-volume (CV) hypothesis, which was proposed by Ramsay (Ramsay, 1952), and Krijgsman and Divaris (Krijgsman and Divaris, 1955). The CV hypothesis postulated that, (1) the total volume of the heart is always the same, (2) ventricle contraction causes a decrease in pressure in the pericardium, (3) the auricles are dilated by the low pericardial pressure, and (4) the low pressure of the auricles increases venous return from the anterior oblique veins (Krijgsman and Divaris, 1955; Beninger and Le Pennec, 2006). To test this hypothesis, it is necessary to measure (a) the changes in the volume of the ventricle, the auricles and the pericardium during the cardiac cycle (1st and 3rd postulates), (b) the changes in the pressure in the ventricle, the auricles and the pericardium (2nd postulate), and (c) the flow direction and velocity of the haemolymph in the ventricle, the anterior aorta, the auricles and the anterior oblique veins (4th postulate). As far as we could determine, pressure changes in the ventricle, the auricles and the pericardium were confirmed for bivalve (*Anodonta anatina*) (Brand, 1972) and gastropod (*Patella vulgata*) (Jones, 1970) species. However, there have been no reports concerning the volume of the heart and the flow of the haemolymph in the heart and adjacent vessels. Indeed, Krijgsman and Divaris (Krijgsman and Divaris, 1955) have discussed the possibility of a reflux of haemolymph to the pericardium through the renopericardial canals, because a backflow would minimize the pressure decrease caused by ventricular contraction. However, for more than 50 years, no one has published on this subject. Therefore, in a future study, we also plan to measure the flow in the pericardium and the renopericardial canals, in addition to the vessels listed above, and further test the CV hypothesis.

Mytilus galloprovincialis Lamarck 1819 was selected as the experimental animal as a lot of related anatomical and physiological information is available (for example Bayne, 1976), and magnetic resonance imaging (MRI) was used as the main experimental tool. MRI is mainly used in the medical field, but MRI studies on invertebrates are gradually increasing (Bock et al., 2001; Herberholz et al., 2004). However, we could not find any MR images of *M. galloprovincialis* in the literature. We needed to obtain measurements from anatomical MR images of the heart and the adjacent vessels and organs, and to compare these with results obtained by conventional histological methods (Prudie, 1887; Borradaile and Potts, 1935; Yamamoto and Handa, 2013). Furthermore, MRI is a precise and non-invasive technique for the measurement of heart rate, for estimating the volume of the ventricle, the auricles and the pericardium, and for determining the direction and velocity of the flow of haemolymph in the heart and adjacent vessels in living mussels. In order to improve the reliability of our conclusions, we conducted our tests of the CV hypothesis under two cardiac functional activity conditions, one more and the other less active. Among several possible environmental factors that may influence this, such as temperature, salinity, oxygen tension, etc., we noticed reports on the effects of aerial exposure, which is expected at low tide (Bayne, 1976). When *M. edulis* was exposed in air, the heart rate reduced and occasionally the heart beat was suppressed completely. This suppression of the heart is not a pathological reaction, but rather a physiological reaction, because the heart rate recovered immediately when the mussel was immersed again after several hours (Helm and Trueman, 1967; Coleman and Trueman, 1971). Therefore, the mussels were

[1]Department of Marine Ecosystem Dynamics, Division of Marine Life Science, Atmosphere and Ocean Research Institute, The University of Tokyo, Kashiwa 277-8564, Japan. [2]Marine Biodiversity Research Program, Institute of Biogeosciences, Japan Agency for Marine-Earth Science and Technology, Yokosuka 237-0061, Japan. [3]Department of Regulatory Physiology, Dokkyo Medical University School of Medicine, Tochigi 321-0293, Japan. [4]Department of Molecular Physiology, National Institute for Physiological Sciences, Okazaki 444-8787, Japan.

*Author for correspondence (yseo@dokkyomed.ac.jp)

Received 18 June 2013; Accepted 12 November 2013

The Journal of Experimental Biology

The Journal of Experimental Biology (2014) doi:10.1242/jeb.092577

List of abbreviations

AV	auriculoventricular valve
CV	constant volume
EDV	end-diastolic volume
EF	ejection fraction
ESV	end-systolic volume
FOV	field of view
I_a	cardiac output via anterior aorta
I_{AP}	filtration from auricles to pericardium
I_{AV}	inflow from auricles to ventricle via auriculoventricular valve
IntraGate	retrospectively self-gated fast low angle shot sequences
I_{PK}	flow from pericardium to kidney via renopericardial canal
I_V	venous return from the anterior oblique vein
MRI	magnetic resonance imaging
N_p	number of phase encoding
PC-MRI	phase-contrast magnetic resonance imaging
PFA	paraformaldehyde
P_P	pressure in the pericardium
SV	stroke volume
T_{1w}-MRI	T_1-weighted gradient-echo magnetic resonance imaging
T_{2w}-MRI	T_2-weighted rapid acquisition with relaxation enhancement magnetic resonance imaging
T_E	echo time
T_R	relaxation delay
V_A	volume of the auricles
V_P	volume of the pericardium
V_V	volume of the ventricle

examined under two conditions: (1) when immersed in synthetic seawater (immersed condition) and (2) when exposed in air (emersed condition). The results obtained under these two conditions were examined to test the CV hypothesis.

RESULTS

MRI of the heart and adjacent vessels

Images from T_2-weighted rapid acquisition with relaxation enhancement (T_{2w})-MRI of living *M. galloprovincialis* are shown in Fig. 1. The detailed structures of the paraformaldehyde (PFA)-fixed mussels are shown in Fig. 2. MR images of the heart and adjacent vessels and organs were compared with the results obtained with conventional histological methods (Prudie, 1887; Borradaile and Potts, 1935; Yamamoto and Handa, 2013). As the shell consists of calcium bicarbonate, no MR signal was detected from the shell, and so the MR images consist of soft tissues and the seawater in the shell. The heart is positioned on the dorsal side near the hinge of the shells, and is pierced by the rectum, as shown in a mid-longitudinal image (Fig. 1A,C). The dorsal part of the heart is surrounded by the shell, and the ventral sides are supported by posterior retractor muscles (Fig. 1B) and the intestine (Fig. 1C). The heart consists of a single ventricle, with a pair of auricles, and these are surrounded by the pericardium. The ventricle has a single outlet to the anterior aorta and two inlets from auricles (Fig. 2A,B). The anterior aorta leaves from the anterior end of the ventricle. The aortic valve is positioned at the root of the anterior aorta (Fig. 2J–L), which is similar to that in *A. anatina* (Brand, 1972), and it prevents backflow from the anterior aorta to the ventricle during diastole of the ventricle. The auriculoventricular (AV) valves are positioned one-third of the way from the anterior end of the ventricle (Fig. 2B,E). The AV valves are dual-flap valves, consisting of anterior and posterior flaps (Fig. 2B,E), which prevent backflow from the ventricle to the auricles during contraction of the ventricle.

The auricles are positioned on the lateral sides of the ventricle. Auricles receive haemolymph from the anterior oblique vein, which is connected at the anterior end of the auricles, and supplies haemolymph to the ventricle via the AV valves (Fig. 1D; Fig. 2B,C,E,G). The posterior ends of the auricles are connected to each other by a communication canal underneath the rectum (Fig. 2C,I). The folding of the auricular wall is also depicted, which is assumed to be the filtration membrane of the haemolymph (Andrews and Jennings, 1993). The pericardium is not a closed cavity. The anterior end of the pericardium is connected with the renopericardial canal, which is connected to the kidney. As shown

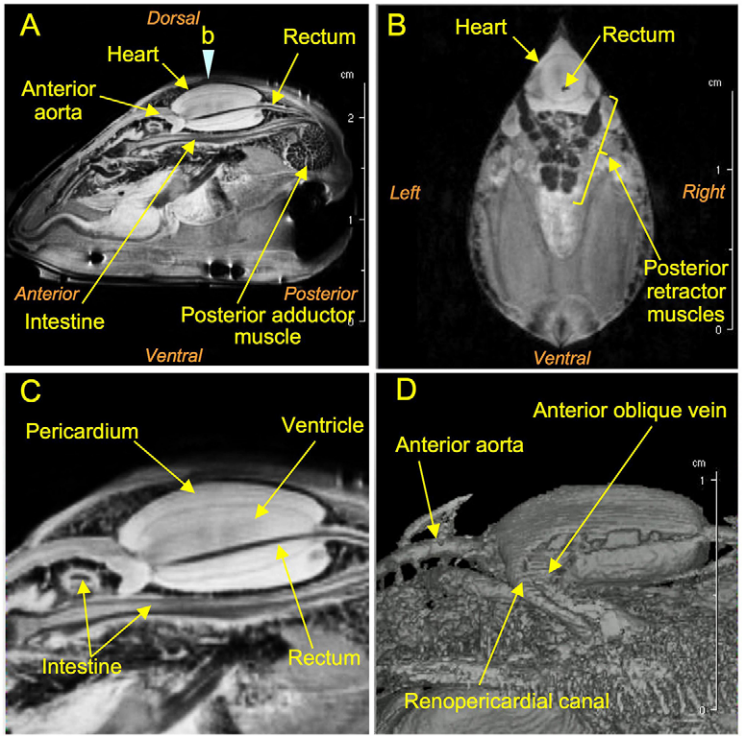

Fig. 1. T_{2w}-weighted magnetic resonance images of living *Mytilus galloprovincialis*. (A) Mid-longitudinal image. The arrowhead labelled b shows the slice position for the transverse image shown in B. (C) Mid-longitudinal image around the heart. (D) 3D reconstructed image of the heart and vessels.

The Journal of Experimental Biology (2014) doi:10.1242/jeb.092577

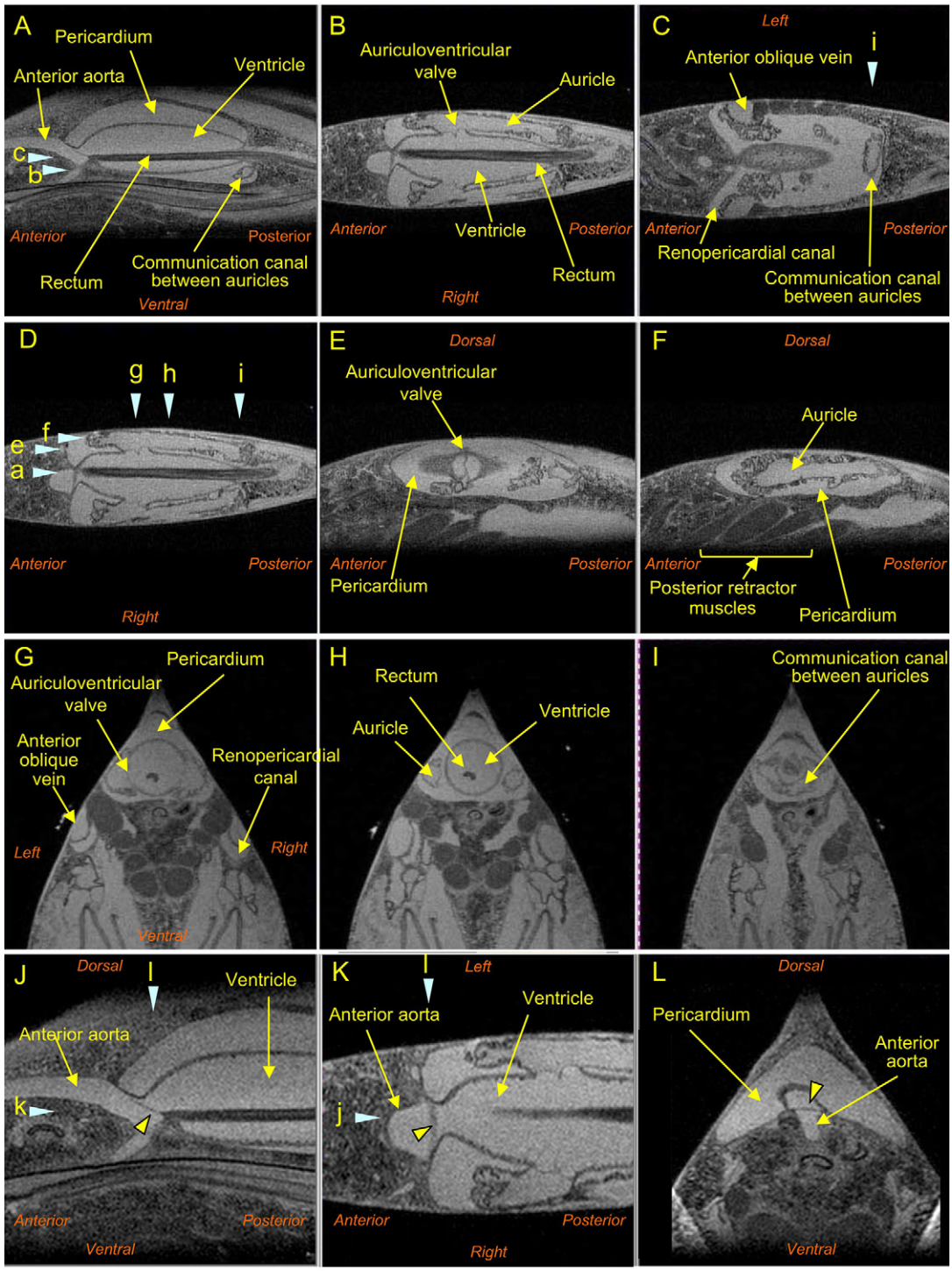

Fig. 2. T_{2w}-MR images of *M. galloprovincialis* fixed by PFA. (A) Mid-longitudinal image around the heart. Arrowheads b and c indicate the slice positions (or planes) of the images shown in B and C, respectively. (B) Horizontal image at the level of the rectum. (C) Horizontal image at the level of the communication canal between the auricles. (D) Horizontal image showing the slice positions of A and E–I using arrowheads labelled a and e–i. (E) Longitudinal image of the left auriculoventricular (AV) valve. (F) Longitudinal image of the left auricle. (G) Transverse image at the AV valve. (H) Transverse image at 1.2 mm posterior to the AV valve. (I) Transverse image at the communication canal between the auricles. (J–L) Mid-longitudinal, horizontal and transverse images around the aortic valve. The yellow arrowhead indicates a flap of the aortic valve. Blue arrowheads, labelled j–l, represent the slice positions of images J–L.

in a 3D reconstructed image (Fig. 1D), the anterior oblique vein and a renopericardial canal run side by side. Therefore, with our procedure, it was possible to obtain images of both of the vessels with a transverse image sliced around the AV valve (Fig. 2G).

As a result, we could obtain MR images showing the ventricle, the auricles and the pericardium, and their inlets and outlets, and also the valves, which are the essential components for the cardiac function of the mussel.

The Journal of Experimental Biology (2014) doi:10.1242/jeb.092577

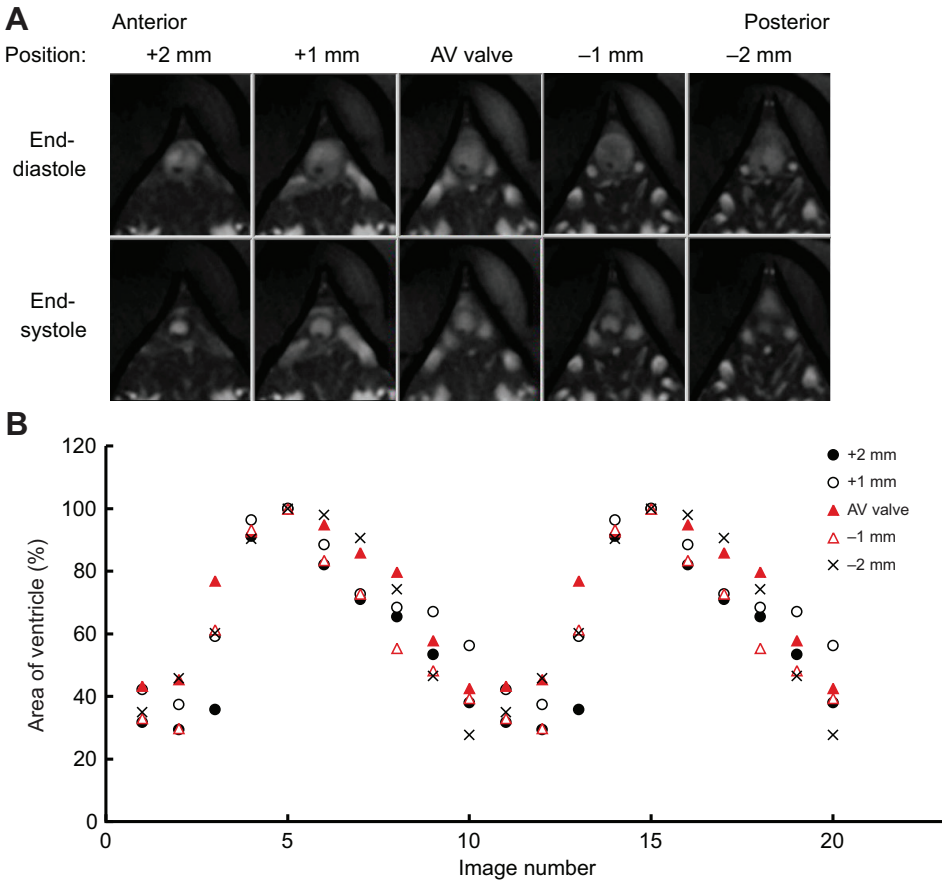

Fig. 3. Changes in ventricular cross-sectional area of *M. galloprovincialis* heart. (A) End-diastole and end-systole transverse images of the heart. Images obtained at five slice positions from 2 mm anterior to 2 mm posterior to the AV valve. (B) Area changes of the ventricles during two cardiac cycles. The ventricle areas were normalized by the area at end-diastole. All of the measurements were conducted within 4.5 h of placing the mussel in the immersed condition.

Heart rate and volume changes in the cardiac cycle

In the immersed condition, *M. galloprovincialis* opened their shells in synthetic seawater at 23°C. Heart rate varied from 0.74 to 1.35 Hz, and the mean (±s.e.m.) value was 1.07±0.09 Hz (N=8). These values are similar to the heart rate (25 beats min^{-1} at 21°C) of resting *M. galloprovincialis*, as observed by impedance pneumography (Braby and Somero, 2006). In the emersed condition, *M. galloprovincialis* shut their shells, and heart rate remained unchanged (0.88±0.05 Hz, mean ± s.e.m., N=5; P>0.05).

As shown in supplementary material Movie 1, a cardiac cycle was divided into 10 frames. As we did not obtain electrocardiographic data, the frame at end-diastole was used as a reference for the timing of the cardiac cycle. Frames of end-diastole and end-systole are shown in Fig. 3A, and changes in the area of the ventricle are shown in Fig. 3B. The results obtained from five slices between 2 mm anterior and 2 mm posterior to the AV valve were almost identical, not only in timing but also in area. The mean area at end-systole was 33.5±3.3% of that of end-diastole (N=5). As shown in Fig. 2, the anterior end of the ventricle was fixed by the anterior aorta, and the posterior end was fixed by the rectum and the wall of the pericardium. Indeed, in the living mussels (Fig. 1C), the wall of the pericardium is clearly shown, and it is not likely that it would move during contraction. Therefore, the length of the long axis of the ventricle is constant during the ventricular contraction. Hence, the volume of the ventricle could be estimated from the area of the ventricle in a single slice. It was also assumed that the volume of the rectum does not change during the heart cycle. For convenience, a slice 1 mm posterior to the AV valve was used for estimation of the cardiac volume. The area of the ventricle, auricles and pericardium was used to calculate the volume of the ventricle, the auricles and the pericardium, respectively.

Changes in the volume of the ventricle, the auricles and the pericardium are shown in Fig. 4. In the immersed condition (Fig. 4A; supplementary material Movie 1), the end-diastolic volume (EDV) and the end-systolic volume (ESV) were 50.2±2.4% and 21.3±3.0% (means ± s.e.m., N=4) of the heart volume, respectively. The stroke volume (SV=EDV–ESV) was estimated as 28.9±2.9% (N=4). The ejection fraction (EF=SV/EDV) was 57.5±5.1% (N=4). The systolic period was longer than the diastolic period, with a ratio of ~3:2. The motion of the auricles showed antiphase, compared with that of the ventricle. The volume of the auricles (V_A) reached a maximum at end-systole (22.1±2.2%, N=4) and a minimum at end-diastole (11.7±1.9%, N=4). The volume of the pericardium (V_P) was minimized at end-diastole (38.1±3.1%, N=4) and maximized at end-systole (56.6±3.1%, N=4). In the emersed condition (Fig. 4B), cardiac motion changed dramatically. EDV, ESV, SV and EF decreased to 30.5±1.8%, 20.1±1.0%, 11.0±1.1% and 33.4±3.7%, respectively (N=5). The systolic period was longer than the diastolic period, with a ratio of ~3:2. The motion of the auricles was in phase with that of the ventricle. V_A reached a maximum at end-diastole (14.5±1.8%, N=5) and showed a minimum at end-systole (11.0±1.1%, N=5). As a result, V_P was minimized at end-diastole (55.1±1.6%, N=5) and maximized at end-systole (68.9±0.7%, N=5). Under the immersed condition, the SV was statistically higher than that observed under the emersed condition (P<0.05).

Flow of haemolymph in the heart and vessels

The flow of haemolymph in the transverse section at the AV valve is summarized in Figs 5 and 6. In the image from T_1-weighted gradient-echo imaging (T_{1w}-MRI), the flow was detected as a higher signal intensity (Fig. 5B), and we could identify vessels, the ventricle and auricles by comparison with an anatomical image obtained by T_{2w}-

The Journal of Experimental Biology (2014) doi:10.1242/jeb.092577

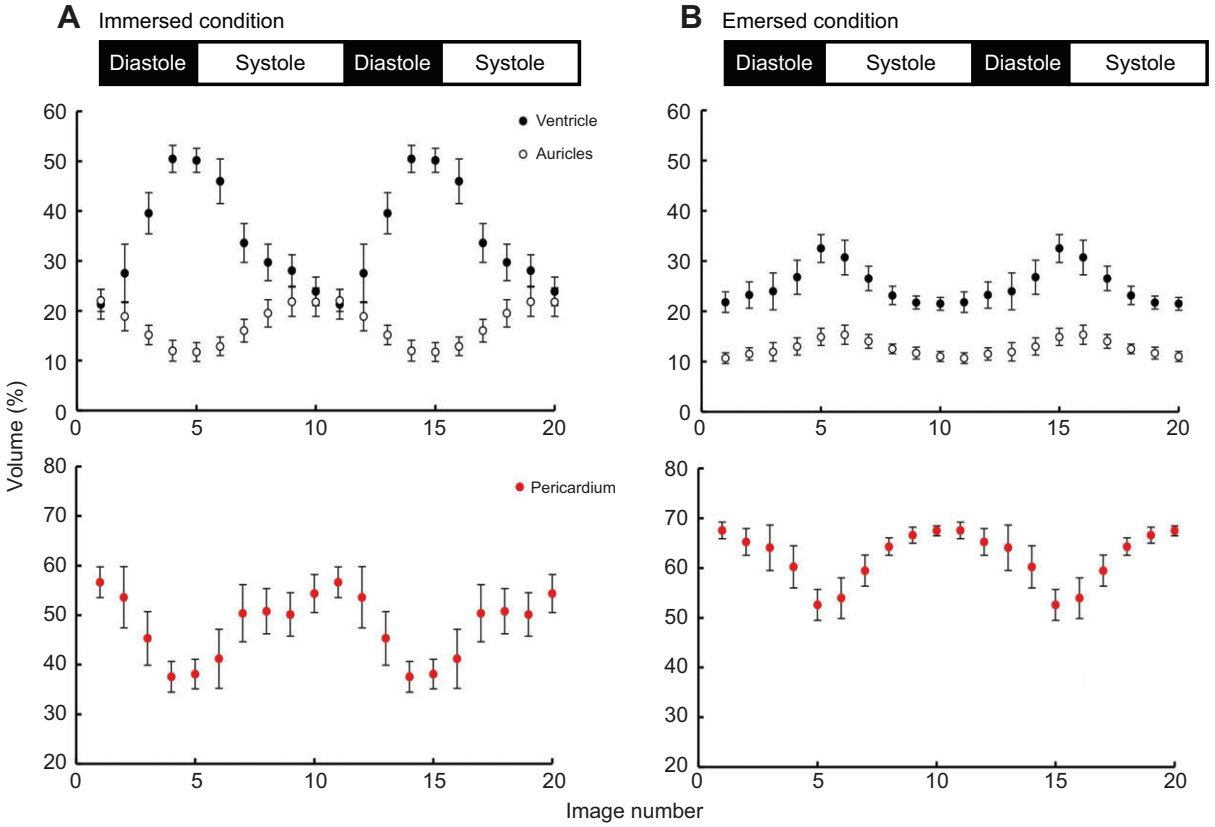

Fig. 4. Changes in the volume of the ventricle, the auricles and the pericardium of *M. galloprovincialis*. (A) A mussel in synthetic seawater (immersed condition) at 23°C. (B) A mussel exposed in air (emersed condition) at 23°C. Volumes were normalized by the total heart volume. The mean and s.e.m. for the volumes from four and five mussels are shown in A and B, respectively. All measurements were conducted from 1 to 2.5 h after setting the mussel under the immersed or emersed condition.

MRI (Fig. 5A). The direction and velocity of flow of haemolymph were detected by a phase-contrast gradient-echo (PC)-MRI. Fig. 5C shows the haemolymph flow at 7.5 mm s^{-1}. The flow of haemolymph in the ventricle, the auricles, the anterior oblique vein, the renopericardial canals and the branchial vessels was detected. In Fig. 5D, the anterior flow and posterior flow are shown in red and blue, respectively. Haemolymph in the anterior oblique vein flows back to the auricle from the vein, while haemolymph in the renopericardial canals flows to the kidney from the pericardium. Slow flow (around 2 mm s^{-1}) is shown in Fig. 6A–D. The flow of haemolymph in the pericardium was not clear in Fig. 5, as the anterior flow velocity was around 2 mm s^{-1} in the pericardium (white arrows in Fig. 6B). In more detail, the flow of haemolymph in the dorsal part of the ventricle was directed to the posterior (yellow arrowhead in Fig. 6C,F), while the flow of haemolymph in the ventral part of the ventricle was directed to the anterior (orange arrowhead in Fig. 6B,F). In a horizontal image of the heart (Fig. 6G), haemolymph flow into the auricle and the ventricle via one of the AV valves is shown as an orange and a yellow arrowhead, respectively (Fig. 6H). As shown in supplementary material Movie 2, at the position of the AV valves, inflow occurred from the AV valves towards the dorsal opposite side.

The flow of haemolymph in the auricles moved in the posterior direction, except for one mussel (data not shown). In that mussel, the inflow via the right AV valve was smaller than that on the left side, suggesting an impairment of the right AV valve. The direction of the haemolymph flow of the right auricle was posterior, and that of the left auricle was anterior. As a result, inflow from the left AV valve increased and may have compensated for the impairment of the right AV valve. Therefore, the haemolymph flow through the communication canal of the auricles might function as a safety circuit to maintain venous return to the ventricle.

DISCUSSION

SV and EF of the heart

This is the first report of measurements of SV and EF of the mussel heart. Cardiac output and SV in the invertebrate have been measured by pulsed Doppler flowmeter and techniques based on the Fick equation, such as the thermodilution technique (Stecyk and Farrell, 2002; Jorgensen et al., 1984). These techniques are advantageous because measurements can be obtained for short-term variations of cardiac functions, compared with MRI. However, using MRI, we were able to measure the exact volume of the heart, and it allowed us to estimate not only SV but also the EF. Under the immersed condition, the SV (29% of the heart volume) and EF (58% of EDV) values were much higher than expected, and EF was similar (60%) to that shown in humans (Boron and Boulpaep, 2004). In *M. galloprovincialis*, the anterior aorta is the only outlet from the ventricle, and the AV valve is positioned one-third of the way from the anterior end of the ventricle (Fig. 2B). The ventricle contracted only on the short axis, as the anterior and posterior ends of the ventricle are anchored at the pericardium wall and the rectum (Fig. 2A). Therefore, it is necessary to pump out haemolymph in the posterior part of the ventricle. Based on the results of the haemolymph flow measurements (Fig. 5 and Fig. 6A–H), the flow of haemolymph in the ventricle was estimated, and is summarized in Fig. 6I,J. The direction of the inflow to the AV valves is not perpendicular to the

The Journal of Experimental Biology (2014) doi:10.1242/jeb.092577

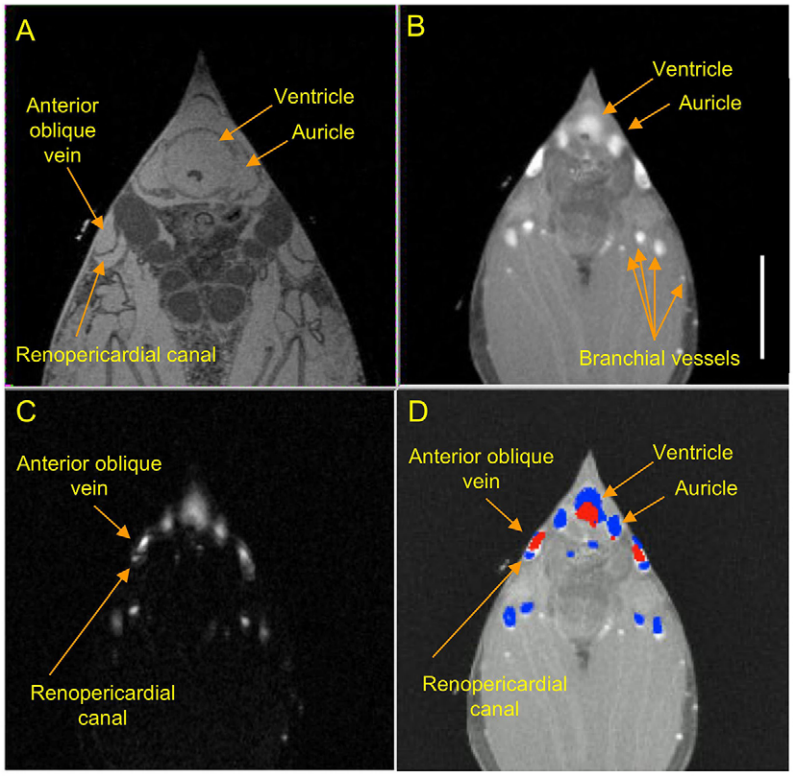

Fig. 5. Haemolymph flow in a transverse section at an *M. galloprovincialis* AV valve. (A) Anatomical image obtained by T_{2w}-MRI. (B) T_{1w}-MR images of living mussels. (C) Vessels observed by phase-contrast (PC)-MRI. (D) Direction of flow at 7.5 mm s^{-1}. Anterior and posterior haemolymph flows are shown in red and blue, respectively. Scale bar, 5 mm.

long axis of the ventricle but, rather, tilted in the posterior dorsal direction. The haemolymph comes from the anterior part of the auricle, which is positioned at the anterior ventral side of the AV valves. Thus, the inflow through the AV valves moves towards the dorsal posterior and the side opposite to that of the ventricle. The streams from the right and left valves may merge together at the posterior end of the ventricle, and are then skewed towards the anterior direction by the inner curvature of the ventricle, and flow in the ventral side of the ventricle to the anterior aorta. These vortices in the haemolymph stream may account for the high EF of the heart, even with a single outlet. Similar vortices in the blood stream were also observed in the human heart (Markl et al., 2011).

CV hypothesis

The CV hypothesis was tested against the four postulates (Krijgsman and Divaris, 1955; Beninger and Le Pennec, 2006). The first postulate is that the total volume of the heart is always the same. We confirmed that the heart volume is always constant, because the wall of the pericardium was imaged clearly even with non-gated T_{2w}-MRI (Fig. 1). The second postulate has already been confirmed by pressure changes in the ventricle, the auricles and the pericardium observed for a bivalve (*A. anatina*) (Brand, 1972) and gastropod (*P. vulgata*) (Jones, 1970) species. Changes in the volume of the pericardium (Fig. 4) also support a decrease in the pressure in the pericardium during systole of the ventricle. The third postulate is that the auricles are dilated by the low pericardial pressure. In the immersed condition, the volume in the auricles was maximized at end-systole and decreased by 10% at end-diastole. As the flow of haemolymph in the auricles was in the posterior direction (Fig. 6C), the haemolymph in the posterior part of the auricles could not return to the AV valve. At least 10% of the haemolymph should be filtered out to the pericardium, which was supported by the fact that we demonstrated anterior flow of the haemolymph in the pericardium around the auricles (Fig. 6B). As shown in Fig. 2, the wall of the auricles has innumerable involutions and folding. Andrews and Jennings (Andrews and Jennings, 1993) found podocytes in the auricular wall of *M. edulis*. Podocytes are now accepted as diagnostic of a site of filtration and the formation of urine. Our results also support the concept that the auricular wall is the filtration site. The filtration of the haemolymph is assumed to be driven by pressure caused by contraction of the ventricle. In order to maintain a constant heart volume, filtration of auricles to the pericardium and the output to the kidney from the pericardium via the renopericardial canals should be the same. Otherwise, the heart volume could not be constant. In the emersed condition, however, the volume in the auricles was minimized at end-systole, even though the volume of the pericardium was maximized at end-systole. Therefore, the third postulate was apparently not applicable to the mussel under the emersed condition.

In order to deal with the remaining questions shown above, and also to test the last postulate, that the low pressure of the auricles increases venous return from the anterior oblique veins, we constructed a model as follows (Fig. 7).

(1) The ventricle has a single outlet to the anterior aorta and a pair of inlets from the auricles via the AV valves. Changes in the volume of the ventricle (ΔV_V) during a period (t) is the difference in the inflow from the auricles (I_{AV}) and the outflow to the aorta (I_a):

$$\Delta V_V = I_{AV} \times t - I_a \times t\,, \quad (1)$$

where I_{AV} and I_a are zero during systole and diastole, respectively.

(2) The auricles receive venous return from the anterior oblique veins (I_V). The auricles transfer haemolymph to the ventricle (I_{AV}), and filtrate haemolymph to the pericardium (I_{AP}). Changes in the volume of the auricles (ΔV_A) can be expressed as follows:

$$\Delta V_A = I_V \times t - I_{AP} \times t - I_{AV} \times t\,, \quad (2)$$

where I_{AV} is zero during systole, and I_{AP} was assumed to be zero during diastole.

The Journal of Experimental Biology (2014) doi:10.1242/jeb.092577

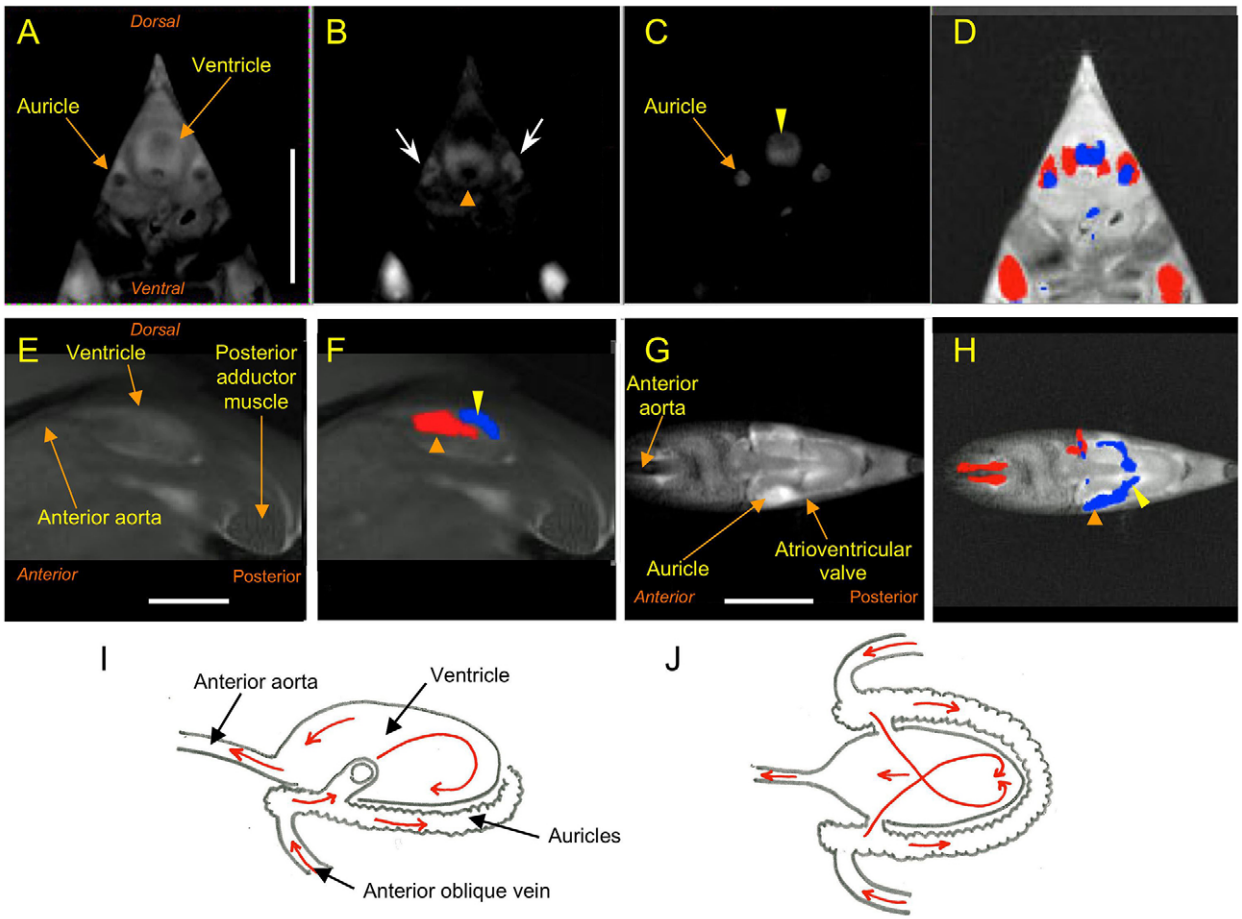

Fig. 6. Haemolymph flow in the heart detected by PC-MRI. (A) Anatomical image of a transverse slice of the heart at 1 mm posterior to the AV valve obtained by T_{1w}-MRI. (B) Anterior flow image obtained at 1.9 mm s^{-1}. (C) Posterior flow image obtained at 1.9 mm s^{-1}. (D) Direction of flow at 1.9 mm s^{-1}. The anterior and posterior haemolymph flow is shown in red and blue, respectively. Haemolymph in the ventral and dorsal side in the ventricle moved in the anterior and posterior direction, respectively. (E) Anatomical image of a mid-longitudinal slice of the heart. (F) Direction of flow at 5.0 mm s^{-1}. Anterior and posterior haemolymph flow is shown in red and blue, respectively. Haemolymph in the ventral side (orange arrowhead) and dorsal side (yellow arrowhead) in the ventricle moved in the anterior and posterior direction, respectively. (G) Anatomical image of a horizontal slice of the heart. (H) Direction of flow at 3.8 mm s^{-1}. Ventral and dorsal haemolymph flow is shown in red and blue, respectively. Venous return to the auricles and inflow into the ventricle are shown by the orange and yellow arrowhead, respectively. (I,J) Schematic diagrams of the haemolymph flow in the ventricle in the longitudinal (I) and horizontal views (J). The direction of the haemolymph stream is shown by red arrows. Scale bars, 5 mm.

(3) The pericardium receives filtrate from the auricles (I_{AP}), and transfers haemolymph to the kidney (I_{PK}). Changes in the volume of the pericardium (ΔV_P) can be expressed as follows:

$$\Delta V_P = I_{AP} \times t - I_{PK} \times t\,, \quad (3)$$

where I_{PK} and I_{AP} were assumed to be zero during systole and the diastole, respectively. Values for ΔV_A, ΔV_V and ΔV_P in the immersed and emersed conditions were used, and the ratio of the systolic period and the diastolic period was set to 3:2. The results of the calculations are summarized in Table 1.

With regard to venous return, in the immersed condition, venous return to the auricles (I_V) was almost constant during the cardiac cycle. Therefore, the low pressure of the auricles during the systolic period could maintain venous return to the auricles. However, in the emersed condition, the cardiac output was reduced to 1/3 that of the immersed condition, and systolic I_V decreased to 1/2 diastolic I_V, because ventricular contraction could not produce enough pressure difference to maintain venous return during the systolic period. In summary, in the emersed condition, because of the increase in the auricular volume during systole, which causes an increase in auricular pressure, the venous return is reduced. In the immersed condition, it is likely that the contraction of ventricle and the associated decrease of pressure in the pericardium maintains the venous return during the systolic period. Therefore, there is no direct relationship between the increase in volume of the auricles and the venous return, which was proposed by the last postulate of the CV hypothesis.

This is the first study to provide an estimation of the filtration rate of haemolymph from the auricles to the pericardium (I_{AP}). In the immersed condition, I_{AP} was 2/3 of the cardiac output (I_a) during systole. Under the emersed condition, I_{AP} was 80% of that observed in the immersed condition, even though I_a decreased to 1/3 that of the immersed condition. This is probably due to the increase in the auricular volume during systole, which causes an increase in auricular pressure, so the filtration rate could be maintained even though there was a smaller decrease of the pressure in the pericardium during systole. In order to maintain the constant volume of the heart, the same amount of haemolymph should be output via the renopericardial canals. Circulation in the renopericardial canals and kidney has attracted little attention (Borradaile and Potts, 1935;

The Journal of Experimental Biology (2014) doi:10.1242/jeb.092577

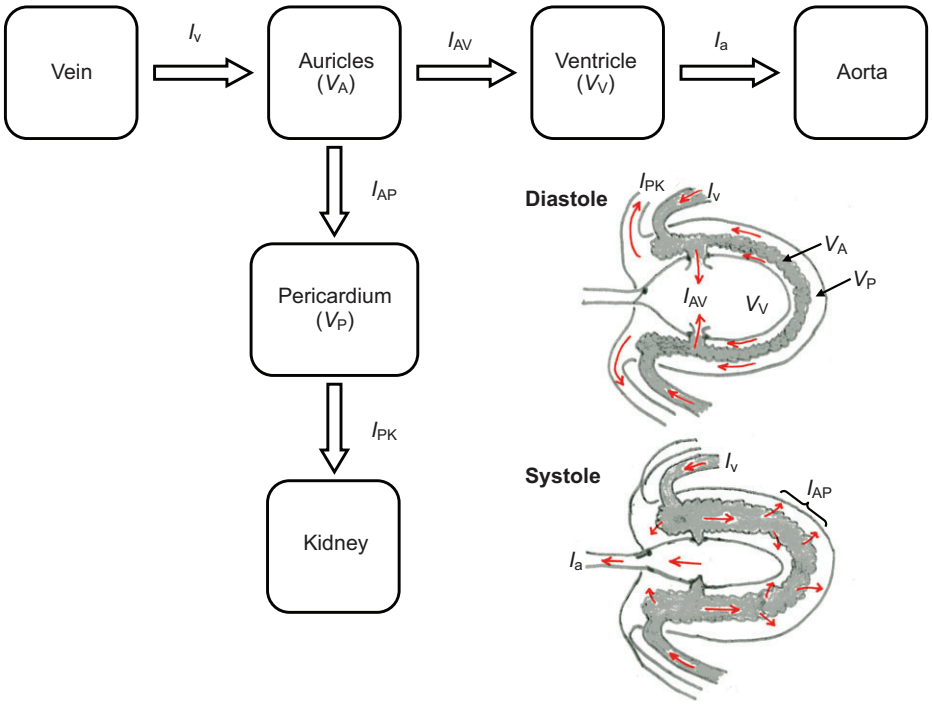

Fig. 7. A model of haemolymph flow and filtration in the heart based on the constant-volume hypothesis. The direction of the haemolymph stream is shown by red arrows. See 'List of abbreviations' for details.

Beninger and Le Pennec, 2006). However, the flow of haemolymph in the renopericardial canals was 2/3 of the aortic output in the immersed condition, and was maintained at the same level under the emersed condition. The kidney and adjacent tissues may prefer a constant supply of haemolymph, as the human kidney does (Boron and Boulpaep, 2004). Therefore, if the ventricle is considered as a high pressure chamber, like the left ventricle in humans, the pericardium may function as a low pressure chamber, like the right ventricle in humans, to maintain homeostasis of the hemolymph. In this simulation, we assumed that output occurred during the diastolic period, as dilatation of the ventricle increases the pressure in the pericardium (P_P), and the increase in pressure causes output to the kidney via the renopericardial canals. We also assumed that back flow in the renopericardial canals during diastole was negligible, because we only detected forward flow to the kidney (Fig. 5D). However, we could not find any valve structure along the renopericardial canals. In order to confirm this speculation, we plan to investigate circulation in the kidney and related tissues in future studies.

In summary, we applied the MRI technique to test the CV hypothesis, and concluded that minor modifications to the CV hypothesis are required. In addition to two postulates of the CV hypothesis: (1) the total volume of the heart is always the same, and (2) ventricle contraction causes a decrease in the pressure in the pericardium, we modified two postulates: (3) the low pericardial pressure maintains venous return from the anterior oblique vein to the auricle, and (4) the pressure difference between the auricle and the pericardium drives filtration of haemolymph through the wall of the auricles. We also added a new postulate: (5) the dilatation of the ventricle is associated with the output of the haemolymph to the kidney via the renopericardial canals.

In addition, the MRI technique promises a massive step forward in our approach to related measurements and our understanding of cardiac functions in the mussel.

MATERIALS AND METHODS

Experimental mussels

Mytilus galloprovincialis were collected on the shore of Kujyukurihama, Chiba, Japan, on 7 July 2012. The mussels were immersed in natural seawater, cooled by ice, and then transported to the laboratory by car within a time period of 3 h. Mussels were also supplied by Hamasui Co. Ltd (Hatsukaichi, Hiroshima, Japan). These mussels were collected from a subtidal area and cultivated using a floating suspended culture off the shore of Miyajima, Hiroshima on 30 October 2012 and 31 March 2013. After collection, the mussels were immersed in natural seawater, cooled by ice, and then transported to the laboratory by a refrigerated transport service, maintained at 10°C, within a time period of 16 h (Cool Ta-Q-BIN, Yamato Transport Co. Ltd, Tokyo, Japan). At the laboratory, the mussels were housed in aerated natural seawater (50 l) in a 90 l bath at room temperature (20–25°C). For convenience, a small number of mussels (around 10) were kept in aerated synthetic seawater (4 l) in a 5 l bath. The natural seawater

Table 1. Estimations of volume changes and haemolymph flows in the ventricle, auricle and pericardium based on the CV hypothesis

	ΔV_V	ΔV_A	ΔV_P	I_a	I_{AV}	I_{AP}	I_{PK}	I_V
	(% total heart volume)			(% total heart volume/heart beat)				
Immersed condition								
Diastole	+29	−10	−19	0	72	0	47	47
Systole	–29	+10	+19	48	0	31	0	48
Emersed condition								
Diastole	+11	+4	–15	0	27	0	37	37
Systole	–11	–4	+15	18	0	25	0	18

CV, constant-volume.

was taken from the sea near Hachijo-jima (Hachijo, Tokyo, Japan), and the synthetic seawater (salinity 3.6%) was made by dissolving a synthetic seawater mixture supplied by Matsuda Inc. (Daito, Osaka, Japan) with distilled water. Half of the volume of the seawater was exchanged every week. Mussels were fed with *Chaetoceros calcitrans* (WDB Environmental and Biological Research Institute, Kaifu, Tokushima, Japan), and 2.5×10^6 cells l^{-1} seawater in the bath were applied at intervals of 1–2 days. The experiments were conducted from 1 to 10 weeks after sampling. A total of 19 mussels were used in this study. The length, height and width of mussels were 34.1±0.4, 20.3±0.3 and 13.0±0.3 mm (means ± s.e.m.), respectively. In order to obtain high spatial resolution MRI, four mussels were fixed with synthetic seawater containing 4% PFA for 1 week at 5°C. All of the animal experiments conducted in this study were carried out under the rules and regulations of the Guiding Principles for the Care and Use of Animals, as approved by the Council of the Physiological Society of Japan.

MRI

The ^{1}H MR images were obtained with ParaVision operating software (version 5.1), using a 7T microimaging system (AVANCE III, Bruker Biospin, Ettlingen, Baden-Württemberg, Germany) equipped with an active shielded gradient (micro2.5) and a 25 mm ^{1}H birdcage radiofrequency coil. The mussels were placed in a plastic tube (barrel of a 30 ml syringe with inner diameter of 22.5 mm; Henke-Sass, Wolf GmbH, Tuttlingen, Baden-Württemberg, Germany) (Fig. 8A). Each mussel was positioned in place using a piece of elastic silicone strip (0.5–1.5 mm thickness and 5–10 mm length), which was inserted at the hinge position of the shell. The elasticity of the silicone strip and the byssus filaments at the ventral edge of the mussel allowed the mussels to open or close their shells. When necessary, two pieces of silicone tubing were cut in half (9 mm outer diameter) and placed beside the shells to immobilize the mussels. The mussels were immersed in 12 ml of synthetic seawater without aeration. When necessary, seawater was drawn from the outlet in the bottom of the tube, and then the mussel was emersed. To prevent drying of the mussels, a piece of wet paper was put on the top of the tube. The temperature of the seawater and the ambient air near the mussels was monitored during the MRI experiments using a fluorescence thermometer (AMOS FX-8000-210, Anritsu Meter, Tokyo, Japan), and the temperature was adjusted to 23±0.3°C (peak-to-peak variance) using a temperature control unit (BCU20, Bruker Biospin, Ettlingen, Baden-Württemberg, Germany). In *M. californianus*, Bayne et al. (Bayne et al., 1976) reported that the heart rate and oxygen tension of the fluid in the mantle cavity stay almost constant for 1–6 h after the start of aerial exposure. Thus, we usually waited for 30–60 min before starting the MRI experiments. Then, during the setting of the slice position, the orientation of mussels and adjustment of the MRI parameters (30 min), the beating of heart and the flow in the vessels were checked at 10 or 20 min intervals. If the heart beat was suppressed completely, we waited up to 2 h for recovery of the heart beat and flow in the vessels. If not, we abandoned the MRI experiment, and replaced the mussel with another one. The series of MRI experiments consisted of (1) detection of the flow of haemolymph in the heart and vessels (2.5 min), (2) measurement of heart rate (5 min), (3) measurement of the motion and volume of the heart (20 min), and/or (4) measurement of the direction and velocity of the flow of haemolymph (10 min). When necessary, sets of measurements from steps 1 to 4 were repeated. The measurements were usually finished within 6 h. In a separate experiment, 3D T_{1w}-MRI (20–40 min) and T_{2w}-MRI (136 min) were measured in order to obtain anatomical information.

The orientation of the planes (Fig. 8B) was defined using the schema described by Norton and Jones (Norton and Jones, 1992). The longitudinal plane was defined as being parallel to the plane defined by the free edges of the bivalves and the hinge. The horizontal plane was defined as being perpendicular to the longitudinal plane and parallel to the basal line of the pericardium, because efferent branchial vessels run parallel to the basal line of the pericardium. The transverse plane was defined as being perpendicular to the longitudinal and horizontal planes. As a convenience, the slice position of the transverse image was measured from the position of the AV valve.

Heart rate and motion of the heart

The heart rate was measured using the motion ghost of the anterior artery or the branchial vessels (Xiang and Henkelman, 1993). Typical parameters for T_{1w}-MRI were as follows: 25.4×25.4 mm field of view (FOV) with a voxel size of 100×100 µm, 1 mm slice thickness, 4 ms echo-time (T_E), 256 phase encodings (N_p), one accumulation. A sinc-shaped pulse (duration 2 ms, flip angle 22.5 deg) was used for excitation. Transverse T_{1w}-MRI of vessels was used to obtain the relaxation delay (T_R), which ranged from 150 to 450 ms. The pulse motion of the haemolymph in the vessel caused periodic motion ghosts in the phase direction of the image. The details of the calculations of the heart rate, and the preliminary experiments conducted using the mouse, are shown in supplementary material Fig. S1.

The heart motion was imaged by retrospectively self-gated fast low angle shot sequences (IntraGate) (Bohning et al., 1990; Bishop et al., 2006), using a transverse or longitudinal slice with a voxel resolution of 100×100 µm and a slice thickness of 1 mm with a combination of T_R/T_E/flip angle=30 ms/6 ms/22.5 deg. Data from 300 images were obtained sequentially for 20 min, and reconstructed into 10 images per cardiac cycle.

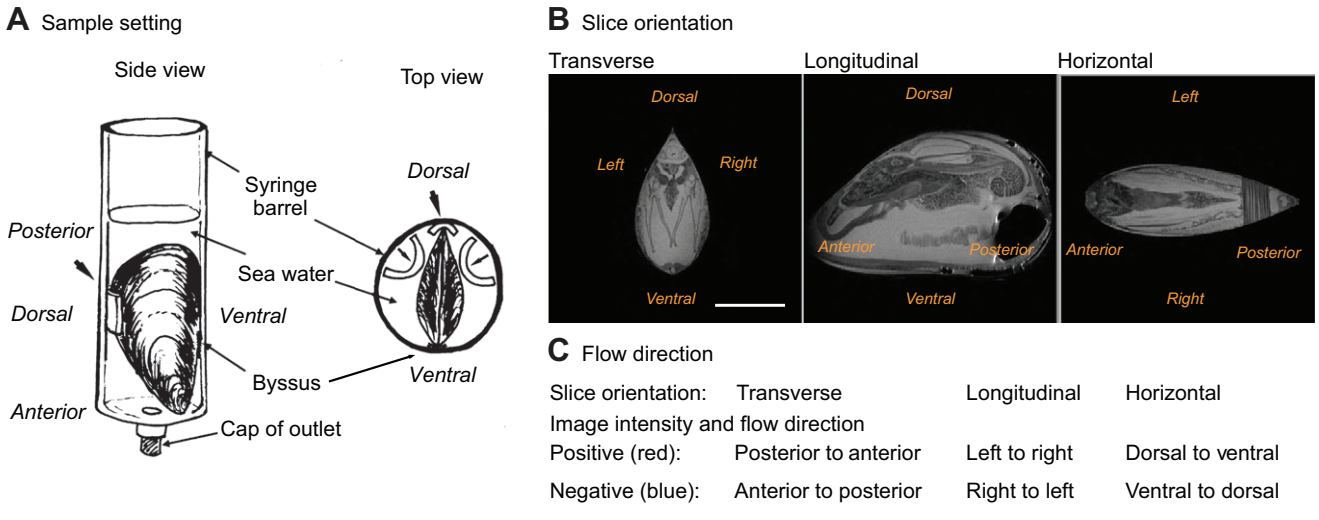

Fig. 8. Mussel settings for the MRI experiments, slice orientation and flow presentation. (A) Sample setting in a plastic tube (inner diameter of 22.5 mm). Arrowheads represent a piece of elastic silicone strip (0.5–1.5 mm thickness and 5–10 mm length), which was inserted at the hinge position of the shell. Short arrows represent pieces of half-cut silicone tubing (9 mm in outer diameter). The mussels were immersed in 12 ml of synthetic seawater without aeration (immersed condition), or seawater drawn out from the outlet in the bottom, and then emersed (emersed condition). The temperature of the seawater or the ambient air was controlled at 23°C. (B) Slice orientation. Scale bar, 10 mm. (C) Flow direction.

Flow of haemolymph

The flow of the haemolymph in the vessels was imaged by the in-flow effect of T_{1w}-MRI (Bock et al., 2001), and the direction and velocity were measured by phase-contrast gradient echo sequences (PC-MRI) (Lotz et al., 2002), using a transverse or horizontal slice with a voxel resolution of 100×100 μm and a slice thickness of 1 mm with a combination of T_R/T_E/flip angle=100 ms/10 ms/45 deg. Eight pairs of velocity encoding gradients were used, with a strength corresponding to a velocity from −22.5 to 30 mm s^{-1} with a 7.5 mm s^{-1} step, and a total image acquisition time of 10 min. When necessary, a slower velocity (1.9–5 mm s^{-1}) could be detected using a higher velocity encoding gradient. As a convenience, the flow direction was defined and presented as shown in Fig. 8C.

Anatomical structure

Anatomical information was obtained by 3D MRI. The imaging parameters used for *in vivo* 3D T_{1w}-MRI were FOV=35.84×35.84×17.92 mm with a voxel size of 140×140×140 μm, a combination of T_R/T_E/flip angle=25 ms/2.5 ms/22.5 deg, and a total image acquisition time of 20–40 min. 3D T_{2w}-MRI was also measured with a voxel size of 140×140×140 μm with a combination of TR/TE/RARE-factor=1000 ms/30 ms/8, and a total image acquisition time of 136 min. For the PFA-fixed mussels, high-resolution 3D T_{2w}-MRI was measured with a voxel size of 55×55×55 μm with a combination of TR/TE/RARE-factor=1500 ms/37.5 ms/8, and a total image acquisition time of 18 h 46 min.

Acknowledgements

The authors would like to thank A. Kinjo and Prof. K. Inoue (AORI, UT) for supplying mussels and providing helpful comments. We would also like to thank R. Murai and H. Okawara (NIPS) for their technical assistance, as well as Prof. S. Kojima (AORI, UT) for his helpful suggestions and encouragement to E.S.

Competing interests

The authors declare no competing financial interests.

Author contributions

E.S., T.M. and Y.S. conceived and designed the experiments; E.S., Y.I.-O., M.M. and Y.S. performed the experiments; E.S., K.O., M.M. and Y.S. analyzed the data; and E.S. and Y.S. wrote the paper. All of the authors approved the final version of the manuscript.

Funding

Parts of this study were supported by grants from the Ministry of Education, Science, and Culture of Japan [grant no. 24659102 to Y.S.], and the Cooperative Study Program of the National Institute for Physiological Sciences [grant no. 106 in 2011 and no. 145 in 2012 to Y.S., T.M. and M.M.].

Supplementary material

Supplementary material available online at
http://jeb.biologists.org/lookup/suppl/doi:10.1242/jeb.092577/-/DC1

References

Andrews, E. B. and Jennings, K. H. (1993). The anatomical and ultrastructural basis of primary urine formation in bivalve molluscs. *J. Mollus. Stud.* **59**, 223-257.

Bayne, B. L. (1976). *Marine Mussels: Their Ecology and Physiology*. Cambridge: Cambridge University Press.

Bayne, B. L., Bayne, C. J., Carefoot, T. C. and Thompson, R. J. (1976). The physiological ecology of *Mytilus californianus* Conrad. 2. Adaptation to low oxygen tension and air exposure. *Oecologia* **22**, 229-250.

Beninger, P. G. and Le Pennec, M. (2006). Structure and function in scallops. In *Scallops: Biology, Ecology and Aquaculture,* 2nd edn. (ed. S. E. Shumway and J. G. J. Parsons), pp. 123-227. Oxford: Elsevier Science.

Bishop, J., Feintuch, A., Bock, N. A., Nieman, B., Dazai, J., Davidson, L. and Henkelman, R. M. (2006). Retrospective gating for mouse cardiac MRI. *Magn. Reson. Med.* **55**, 472-477.

Bock, C., Frederich, M., Wittig, R.-M. and Pörtner, H.-O. (2001). Simultaneous observations of haemolymph flow and ventilation in marine spider crabs at different temperatures: a flow weighted MRI study. *Magn. Reson. Imaging* **19**, 1113-1124.

Bohning, D. E., Carter, B., Liu, S. S. and Pohost, G. M. (1990). PC-based system for retrospective cardiac and respiratory gating of NMR data. *Magn. Reson. Med.* **16**, 303-316.

Boron, W. F. and Boulpaep, E. L. (2004). *Medical Physiology*. London: Saunders.

Borradaile, L. A. and Potts, F. A. (1935). *The Invertebrata: A Manual For the Use of Students,* 2nd edn. Cambridge: Cambridge University Press.

Braby, C. E. and Somero, G. N. (2006). Following the heart: temperature and salinity effects on heart rate in native and invasive species of blue mussels (genus *Mytilus*). *J. Exp. Biol.* **209**, 2554-2566.

Brand, A. R. (1972). The mechanism of blood circulation in *Anodonta anatina* (L.) (Bivalvia, Unionidae). *J. Exp. Biol.* **56**, 361-379.

Coleman, N. and Trueman, E. R. (1971). The effect of aerial exposure on the activity of the mussels *Mytilus edulis* L. and Modiolus modiolus (L.). *J. Exp. Mar. Biol. Ecol.* **7**, 295-304.

Helm, H. H. and Trueman, E. R. (1967). The effect of exposure on the heart rate of the mussel, *Mytilus edulis* L. *Comp. Biochem. Physiol.* **21**, 171-177.

Herberholz, J., Mims, C. J., Zhang, X., Hu, X. and Edwards, D. H. (2004). Anatomy of a live invertebrate revealed by manganese-enhanced Magnetic Resonance Imaging. *J. Exp. Biol.* **207**, 4543-4550.

Jones, H. D. (1970). Hydrostatic pressures within the heart and pericardium of *Patella vulgata* L. *Comp. Biochem. Physiol.* **34**, 263-272.

Jorgensen, D. D., Ware, S. K. and Redmond, J. R. (1984). Cardiac output and tissue blood flow in the abalone, *Haliotis cracherodii* (Mollusca, Gastropoda). *J. Exp. Zool.* **231**, 309-324.

Krijgsman, B. J. and Divaris, G. A. (1955). Contractile and pacemaker mechanism of the heart of molluscs. *Biol. Rev. Camb. Philos. Soc.* **30**, 1-39.

Lotz, J., Meier, C., Leppert, A. and Galanski, M. (2002). Cardiovascular flow measurement with phase-contrast MR imaging: basic facts and implementation. *Radiographics* **22**, 651-671.

Markl, M., Kilner, P. J. and Ebbers, T. (2011). Comprehensive 4D velocity mapping of the heart and great vessels by cardiovascular magnetic resonance. *J. Cardiovasc. Magn. Reson.* **13**, 7.

Norton, J. H. and Jones, G. W. (1992). *The Giant Clam: An Anatomical and Histological Atlas*. Canberra, ACT: Australian Centre for International Agricultural Research.

Prudie, A. (1887). *The Anatomy of the Common Mussels (Mytilus latus, Edulis and Magellanicus).* Wellington, New Zealand: Colonial Museum and Geological Survey Department. (Republished in 2012 by Ulan Press.)

Ramsay, J. A. (1952). *A Physiological Approach to the Lower Animals*. Cambridge: Cambridge University Press.

Stecyk, J. A. W. and Farrell, A. P. (2002). Cardiorespiratory responses of the common carp (*Cyprinus carpio*) to severe hypoxia at three acclimation temperatures. *J. Exp. Biol.* **205**, 759-768.

Xiang, Q. S. and Henkelman, R. M. (1993). K-space description for MR imaging of dynamic objects. *Magn. Reson. Med.* **29**, 422-428.

Yamamoto, K. and Handa, T. (2013). Structure of ctenidium in the Mediterranean blue mussel *Mytilus galloprovincialis*. *J. Natl. Fish. Univ.* **61**, 123-142.

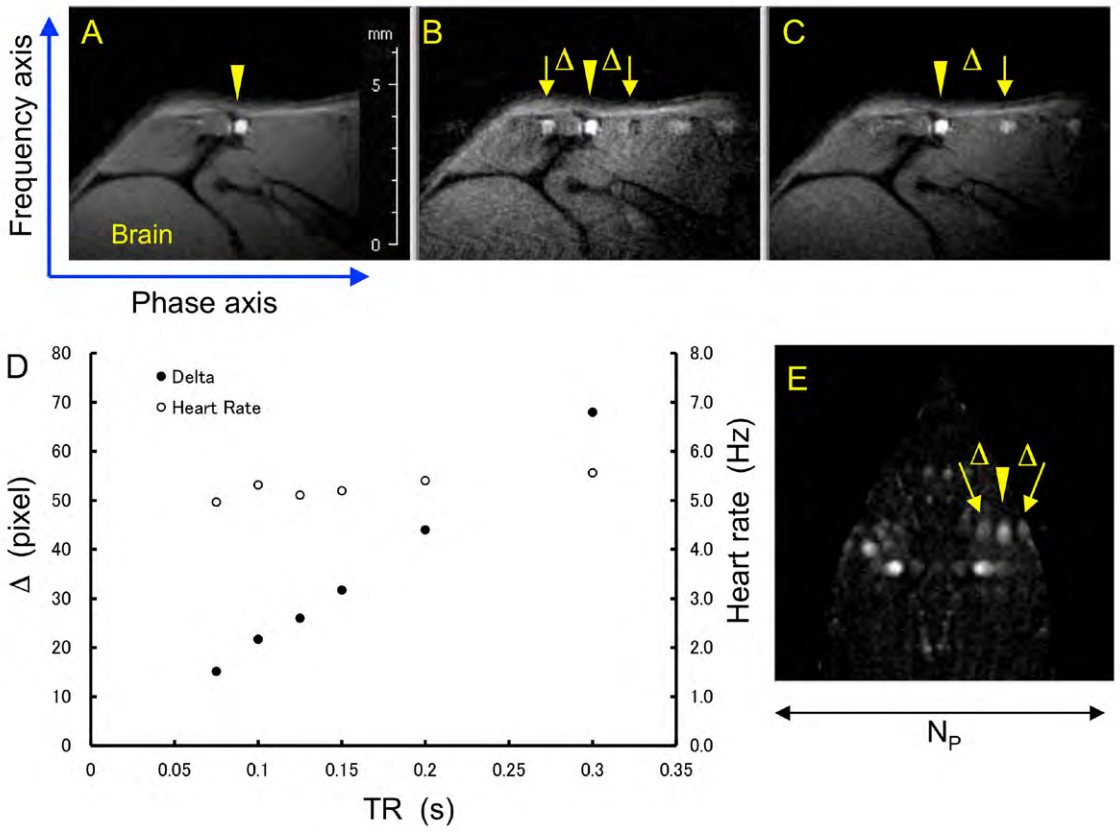

Fig. S1. Measurement of the heart rate obtained from the motion ghost caused by periodic pulsed motion of the haemolymph in the vessel by T_{1w}-MRI. (A–D) Preliminary experiments were conducted using the internal carotid artery (ICA) of the mouse. (A) Coronal image of the left side of the head of the mouse with motion artifact compensation. The position of the ICA is shown by an arrow head. (B-C) Coronal image without motion artifact compensation. The periodic motion ghost was measured at T_R 0.1 s (B) and 0.15 s (C). Arrows show the position of the ghost along the phase direction of the image. (D) The interval of the motion ghost (Δ) and the estimated heart rate (ω beats s^{-1}) were obtained from the following equation:

$$\omega = 2\pi \Delta / (T_R N_p)$$

where N_p is number of phase encodings. The Δ values of the ICA increased linearly when T_R was increased from 75 ms to 250 ms. The observed heart rate, 5.3 ± 0.2 beats s^{-1}, was in agreement with the heart rate obtained by electrocardiography (300 beats min^{-1}). (E) Transverse image of the branchial vessel of *M. galloprovincialis.* The position of a branchial vessel and its ghosts are shown by an arrow head and arrows, respectively. From Δ (8 pixels), N_p (256) and TR (0.15 s), the heart rate was calculated as 1.3 beats s^{-1}.

Movie 1. An Intragate MR movie of the cardiac cycle with a transverse image at 1 mm posterior to the AV valve. Four cardiac cycles at 10 frames/beat are shown.

Movie 2. An Intragate MR movie of the cardiac cycle with a transverse image at the position of the AV valve. Four cardiac cycles at 10 frames/beat are shown.